



Investigation on miscibility, thermal, crystallographic diffraction and dynamic-mechanical properties of poly(vinyl alcohol)/poly(vinylpyrrolidone)/zirconium phosphate nanocomposites

Daniela F. S. Freitas¹ · Gabriela C. Mattos¹ · Luis C. Mendes¹

Received: 7 October 2019 / Accepted: 18 March 2020 / Published online: 13 May 2020
© Akadémiai Kiadó, Budapest, Hungary 2020

Abstract

This work approaches the effects of a synthetic nanofiller on poly(vinyl alcohol)/poly(vinylpyrrolidone)/zirconium phosphate (PVA/PVP/ZrP) nanocomposites searching its future application as control drug delivery. ZrP was synthesized by reaction of phosphoric acid and zirconium (IV) oxide chloride 8-hydrate ($\text{ZrOCl}_2 \cdot 8\text{H}_2\text{O}$). Nanocomposites with fixed amount of ZrP (2 mass%) and three different blend proportions were studied. Structural, miscibility, thermal, and crystallographic diffraction and dynamic-mechanical characteristics were assessed. For all nanocomposites, wide-angle X-ray diffraction showed changes for the ZrP diffraction pattern with the amount of PVA leading to an intercalated structure. Infrared spectroscopy (FTIR) revealed strong interaction between PVA and ZrP. It was observed that ZrP collaborates with the improvement in PVA thermal stability. For all nanocomposites, PVA crystallinity degree, cold crystallization, and melting temperatures were reduced. Storage modulus increased showing reinforcing action of ZrP. Miscibility study by dynamic mechanical analysis induced to infer that the PVP-rich nanocomposite formed a polymeric miscible system.

Keywords Zirconium phosphate · Nanocomposites · Poly(vinylpyrrolidone) · Poly(vinyl alcohol) · Intercalation

Introduction

The increase in world polymer consumption led to a demand for better systems to provide products with better performance, which directed to the development of multiphase systems like blends, alloys, and composites. The identification of blends was not always possible, as some polyolefins suppliers, for example, usually mix polymers to maintain polymer specification and these are sold as single resins. The reason for blending emerged from a necessity to toughen rigid resins or increase rigidity of soft polymers. Over the years, the studies to understand the behavior of polymer blends intensified in a way to provide materials with lower cost [1, 2].

Poly(vinyl alcohol) (PVA) is a synthetic polymer synthesized by chemical modification of poly(vinyl acetate) with

outstanding properties like non-toxicity, biocompatibility, water solubility, and chemical and thermal stability [3]. Its application as a paper coating, adhesives, and colloid stabilizer is widespread [4]. With the advent of the nanotechnology and due to its biologic compatibility, PVA has been studied a lot in the development of systems devoted to control drug delivery. Additionally, it finds application in the medical sector as dialysis membranes, wound dressing, artificial skin, cardiovascular devices, and so on [5–7].

Poly(N-vinyl-2-pyrrolidone) (PVP) is also a synthetic polymer. It is a nonionic vinyl polymer with amphiphilic character due to its chemical structure with hydrocarbon main chain and pyrrolidone pedant group [8]. Indeed, it imparts special characteristics and unique combination of properties such as good solubility in water and organic solvents, great interaction with several organic and inorganic compounds, high biocompatibility, and non-toxicity among others. Szczerba et al. described the strong interaction between PVP and smectites. However, the nanofiller addition may reduce or even avoid polymer interaction [9]. PVP has been widely used as additive in applications such as medical health, polymeric modifier, and excipients in pharmaceuticals [4, 6, 10, 11]. Also, it is used in studies for

✉ Luis C. Mendes
lcmendes@ima.ufrj.br

¹ Instituto de Macromoléculas Professora Eloisa Mano, Universidade Federal do Rio de Janeiro, Av Horacio Macedo 2030, CT - Bloco J, Ilha Do Fundão, Rio de Janeiro, RJ 21941-598, Brazil

topical skin application for transdermal drug delivery, drug release control, and drug diffusion [6, 7, 12].

It is quite known the compatibility between PVA and PVP, particularly for production of new biomaterials because of its good compatibility. Pedant pyrrolidone ring attached to PVP structure is a proton-accepting group and thus may interact with PVA hydroxyl leading to the hydrogen-bonding formation. Also, both polar side groups in polymer chain allow solubility in water. These characteristics suggest that PVA/PVP system may be miscible. However, it is not clear the effect of the insertion of nanofillers, once it may lead to a strong linkage with any of the polymers or avoid chain interaction between them [8, 13, 14].

The study of polymer nanocomposites is more and more disseminated in the academic and industrial sectors. In this context, the nanoparticles assume an important role to solve demands in the short term and long term. Their feasible structure, size, stability, and dispersion in the polymeric matrix are responsible for the improvement of properties and performance. Thus, the synergism between polymer and filler creates hybrids and advanced materials with new abilities [15–18]. Similar to phyllosilicates, synthetic lamellar phosphates gained importance as a substitute to natural clays, which the α -zirconium phosphate (α -ZrP) was the pioneer, and it has been intensively studied in the last years due to the intrinsic properties. Its crystalline structure is arranged by overlapped layers of the zirconium atoms connected to the oxygen and phosphate groups, where among interlayer the interlayer sheets, P–OH acid groups are available to accomplish direct Bronsted acid–base reaction with basic compounds, like amines. The degree of saturation is responsible for the arrangement of the molecules inside the phosphate layers that possess high aspect ratio and high cation exchange capacity (CEC). With the insertion of guest molecules, intercalated and exfoliated structures are reached promoting interaction enhancement between polymers and the nanofiller [19–23].

Thinking as a promising material for drug delivery system, we developed PVA/PVP/ZrP nanocomposites. Herein, the focus was to investigate the effect of the ZrP nanofiller on the miscibility, thermal, and crystallographic diffraction and dynamic-mechanical properties of the nanocomposites. Detailed characterization was performed.

Experimental

Materials

Poly(vinyl alcohol) (PVA) (99% hydrolyzed; density of 1269 kg m^{-3}) and poly(N-vinyl-2-pyrrolidone) (PVP) (average mol. Wt. 40,000) both from Sigma-Aldrich were used as

received. Phosphoric acid (H_3PO_4) and zirconium (IV) oxide chloride 8-hydrate ($\text{ZrOCl}_2 \cdot 8\text{H}_2\text{O}$) were provided by Vetec.

Synthesis of layered zirconium nanofillers (ZrP)

According the method described and used by Albert et al. and Mendes et al., nano-zirconium phosphate was synthesized. With P/Zr ratio equal 18, a mixture of phosphoric acid (H_3PO_4) and zirconium (IV) oxide chloride 8-hydrate ($\text{ZrOCl}_2 \cdot 8\text{H}_2\text{O}$) was kept under reflux, during 48 h; sequentially, the precipitated was centrifuged, washed with distilled water until pH of 6, frozen at $-80 \text{ }^\circ\text{C}$, during 24 h and finally lyophilized for 4 days [20, 24].

Nanocomposites preparation

Water solution blends of PVA and PVP (PVA/PVP) at different mass ratios (30/70, 50/50, and 70/30 mass/mass%) were prepared dissolving separately PVA and PVP in deionized water, at $60 \text{ }^\circ\text{C}$, with stirring, until complete dissolution. Following, the solutions were mixed. After that, a certain amount of ZrP was dispersed in deionized water in order to produce nanocomposites with 2 mass% of nanofiller. The ZrP dispersion was added dropwise to the blend solution, kept under stirring for 40 min. Nanocomposite films were obtained by pouring its solution onto Petri dishes, dried overnight in an oven, at $60 \text{ }^\circ\text{C}$. For comparison, PVA and PVP films were prepared.

Thermogravimetry/derivative thermogravimetry (TG/DTG)

Thermogravimetric curve was obtained using a TA Q500 thermogravimetric analyzer from 0 to $700 \text{ }^\circ\text{C}$, at $10 \text{ }^\circ\text{C min}^{-1}$, using nitrogen as carrying gas. T_{50} (temperature of 50% loss mass) and T_m (temperature of maximum degradation rate) were detected.

Differential scanning calorimetry (DSC)

According to the ASTM D3418 and assisted by TA Instruments Q1000 differential scanning calorimeter (DSC), the calorimetric properties were determined. First, the sample was heated from 0 to $240 \text{ }^\circ\text{C}$, at heating rate of $10 \text{ }^\circ\text{C min}^{-1}$ and kept for 1 min in order to eliminate the thermal history. After that, a cooling cycle at equipment maximum rate was carried out. Following, a second heating cycle was performed at the same conditions as the first one, and then, a second cooling cycle at $10 \text{ }^\circ\text{C min}^{-1}$ was conducted. Finally, a third heating cycle similar to the first one was carried out. When possible, the cold crystallization temperature (T_c) and crystalline melting temperature (T_m) were taken at second cooling and third heating cycles, respectively. Degree of

crystallinity (X_c) was calculated considering the enthalpy of fusion (ΔH_m) of the third heating cycle applying the Eq. (1) [25]. ΔH_m ($J g^{-1}$) is the experimental melting enthalpy, ΔH_m° ($J g^{-1}$) is the melting enthalpy of PVA 100% crystalline equal to $152 J g^{-1}$ [26, 27], and ϕ is the filler mass fraction in the nanocomposites. The value was normalized according to the blend composition and filler content.

$$X_c = \frac{\Delta H_m}{(1 - \phi)\Delta H_m^\circ} \times 100 \quad (1)$$

Wide-angle X-ray diffraction (WAXD)

The WAXD analysis was carried out in a Rigaku Ultima IV diffractometer with $CuK\alpha$ radiation (wavelength = 1.5406 \AA), at 40 kV, 20 mA, and 2θ varying between 2 and 35° (resolution of 0.05°). The interlamellar spacing was calculated according to the Bragg's relation ($\lambda = 2d \sin \theta$) and the crystal size by Scherrer equation.

Dynamic mechanical analysis (DMA)

Storage modulus (E'), loss modulus (E''), and tangent delta ($\tan \delta$) were determined using a TA Instruments Q800 instrument in tension film mode through rectangular specimen with dimensions of $13 \times 9 \times 0.45 \text{ mm}$, from -50 to $200^\circ C$, heating rate of $3^\circ C \text{ min}^{-1}$ and frequency of 1 Hz. Fox's equation (Eq. 2) was used to help the evaluation of the blend glass transition temperature (T_g) where w_1 , w_2 , T_{g1} , and T_{g2} are PVA and PVP polymer mass fractions and their glass transition temperatures, respectively [28].

$$\frac{1}{T_g} = \frac{w_1}{T_{g1}} + \frac{w_2}{T_{g2}} \quad (2)$$

In order to assess the miscibility degree of the polymer blends, Eqs. (3) and (4) are adapted from the works of Santana et al. and Al-Jabareen et al. on PET/PC and PC/ABS blends, respectively [29–31]. The abbreviation definitions of Eqs. (3) and (4) are summarized in Table 1.

$$w'_{PVA} = \frac{T_{gPVA}(T_{gPVP} - T'_{gPVP})}{T'_{gPVP}(T_{gPVP} - T_{gPVA})}; \quad w''_{PVP} = \frac{T_{gPVP}(T''_{gPVA} - T_{gPVA})}{T''_{gPVA}(T_{gPVP} - T_{gPVA})} \quad (3)$$

$$\epsilon_{PVA} = \frac{w'_{PVA} \times x_{PVP}}{(w'_{PVA} \times x_{PVP}) + ((1 - w'_{PVP}) \times x_{PVA})} \times 100; \quad (4)$$

$$\epsilon_{PVP} = \frac{w''_{PVP} \times x_{PVA}}{(w''_{PVP} \times x_{PVA}) + ((1 - w'_{PVA}) \times x_{PVP})} \times 100$$

Infrared spectroscopy (FTIR)

FTIR analysis was performed in a Perkin Elmer equipment model Frontier using ATR assembly mode, ranging from 4000 to 500 cm^{-1} , 60 scans, and 4 cm^{-1} of resolution.

Results and discussion

Wide-angle X-ray diffraction

Figure 1 presents the X-ray diffraction patterns of PVA, PVP, ZrP, and PVA/PVP/ZrP nanocomposites. PVA diffractogram exhibited hkl diffraction angle at $2\theta = 19.8^\circ$ (110) with crystal size of 63.79 \AA . This plane was attributed to the extended crystallites of zig-zag planar chain direction as reported by Eisa et al. [15]. PVP diffraction patterns showed a halo characteristic of amorphous polymer analogous to found by Mendes and collaborators [32]. ZrP presented 2θ angle at 12.35° (hkl 002) with d_{spacing} of 7.16 . These parameters are similar to those found in several works on ZrP synthesis and characterization [33–35]. Concerning to diffraction patterns of the nanocomposites, alterations of PVA and ZrP hkl planes were noticed (Table 2). Sharply PVA diffraction peak decreased intensity, and its crystal size showed tendency to diminish. ZrP basal plane (hkl) changed (see black arrows). For the nanocomposite PVA/PVP/ZrP (70/30/2 mass/mass/mass%), the pristine ZrP hkl plane was completely destroyed and new diffraction angle appeared at $2\theta = 11.3^\circ$. Also, ZrP original basal plane was damaged for the nanocomposites

Table 1 Abbreviation definitions of Eqs. 3 and 4

| Abbreviation | Definition |
|------------------|---|
| T_{gPVA} | Glass transition temperature of pristine PVA in Kelvin degree |
| T_{gPVP} | Glass transition temperature of pristine PVP in Kelvin degree |
| T''_{gPVA} | Glass transition temperature of PVA-rich phase in Kelvin degree |
| T'_{gPVP} | Glass transition temperature of PVP-rich phase in Kelvin degree |
| w'_{PVA} | Estimated apparent mass fraction of PVA in the PVP-rich phase |
| w''_{PVP} | Estimated apparent mass fraction of PVP in the PVA-rich phase |
| ϵ_{PVA} | PVA participation effectiveness degree on the PVP-rich phase |
| ϵ_{PVP} | PVP participation effectiveness degree on the PVA-rich phase |

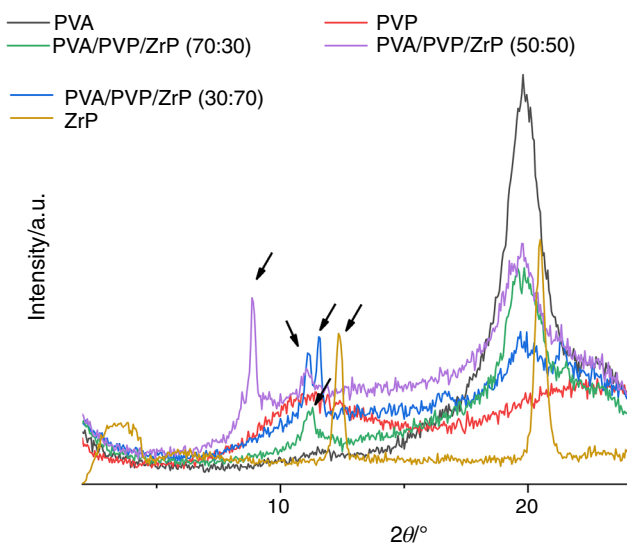


Fig. 1 WAXD patterns of the PVA, PVP, ZrP, and nanocomposites

Table 2 Crystallographic data of PVA and ZrP/pristine and in the nanocomposites

| | $2\theta/^\circ$ | $d_{\text{spacing}}/\text{\AA}$ | Crystal size/ \AA |
|-----------|--------------------|---------------------------------|----------------------------|
| ZrP | 12.35 | 7.16 | 391 |
| PVA | 19.8 | — | 63.79 |
| 70/30/ZrP | PVA—19.8 | — | 61.22 |
| | ZrP—11.3 | 7.82 | — |
| 50/50/ZrP | PVA—19.8 | — | 47.09 |
| | ZrP—8.85 and 11.05 | 9.98 and 8.00 | — |
| 30/70/ZrP | PVA | — | — |
| | ZrP—11.1 and 11.55 | 7.96 and 7.65 | — |

PVA/PVP/ZrP (50/50/2 and 30/70/2 mass/mass/mass%) showing new diffraction angles at (8.85 and 11.05°) and (11.1 and 11.55°), respectively. Gardolinski et al. accomplished the pre-intercalation of kaolinite with dimethyl sulfoxide (DMSO). Its structure was partially destroyed and a new intercalated plane was observed at low angle [36]. Nylon-6 montmorillonite nanocomposite kept its morphology independent on the preparation process as reported by Fong et al. [37]. Wu and co-workers [38] pointed out the action of saponite and montmorillonite on the nylon-6 polymorphic behavior. In their work on the montmorillonite/mica filling up poly (lactic acid) nanocomposites, Chang et al. [39] reported the absence of exfoliation. The occurrence of interaction between hydroxyl groups along the PVA chain and P–OH groups attached to the ZrP structure could explain the damage of the original ZrP diffraction angle and the appearance of new crystallographic plane at low angle. ZrP possesses lamellar arrangement with nanometric dimension, and into its interlamellar region, P–OH groups are attached. During the nanocomposite preparation, blend solution permeated the filler galleries. We believe that there is a competition between PVP and ZrP to get hydrogen bond with PVA. Although studies indicate that PVP could form hydrogen bond with PVA, herein we supposed that preferentially OH side groups of PVA interacted with P–OH of ZrP leading to the damage of the phosphate crystalline organization. It is reasonable to infer that part of PVA is placed inside of ZrP galleries. A schematic representation of hydrogen bond formation between OH groups attached in PVA and ZrP is shown in Fig. 2.

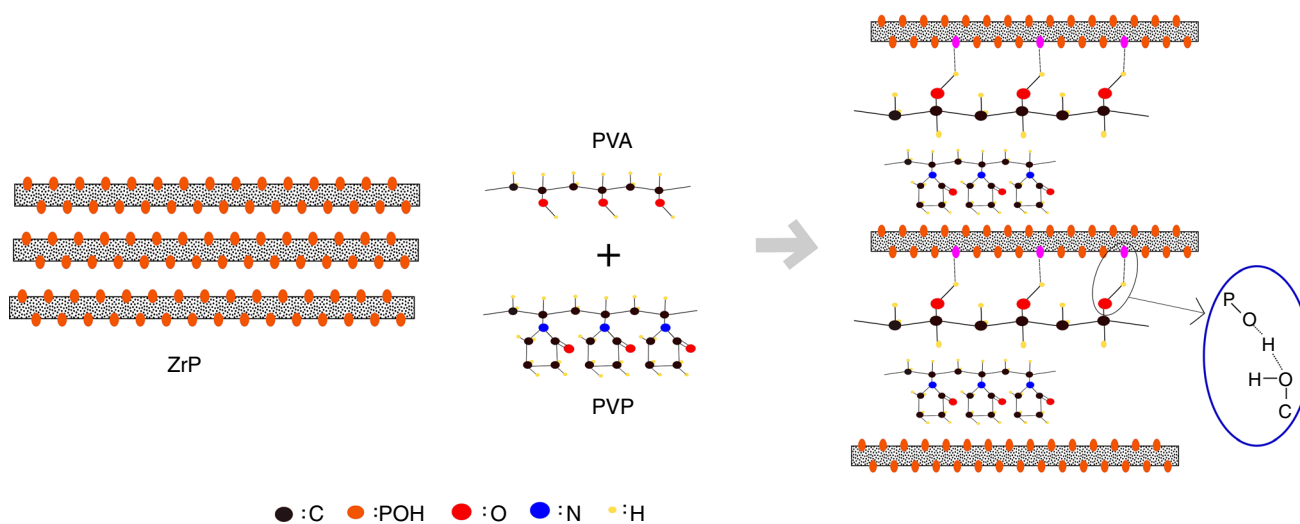
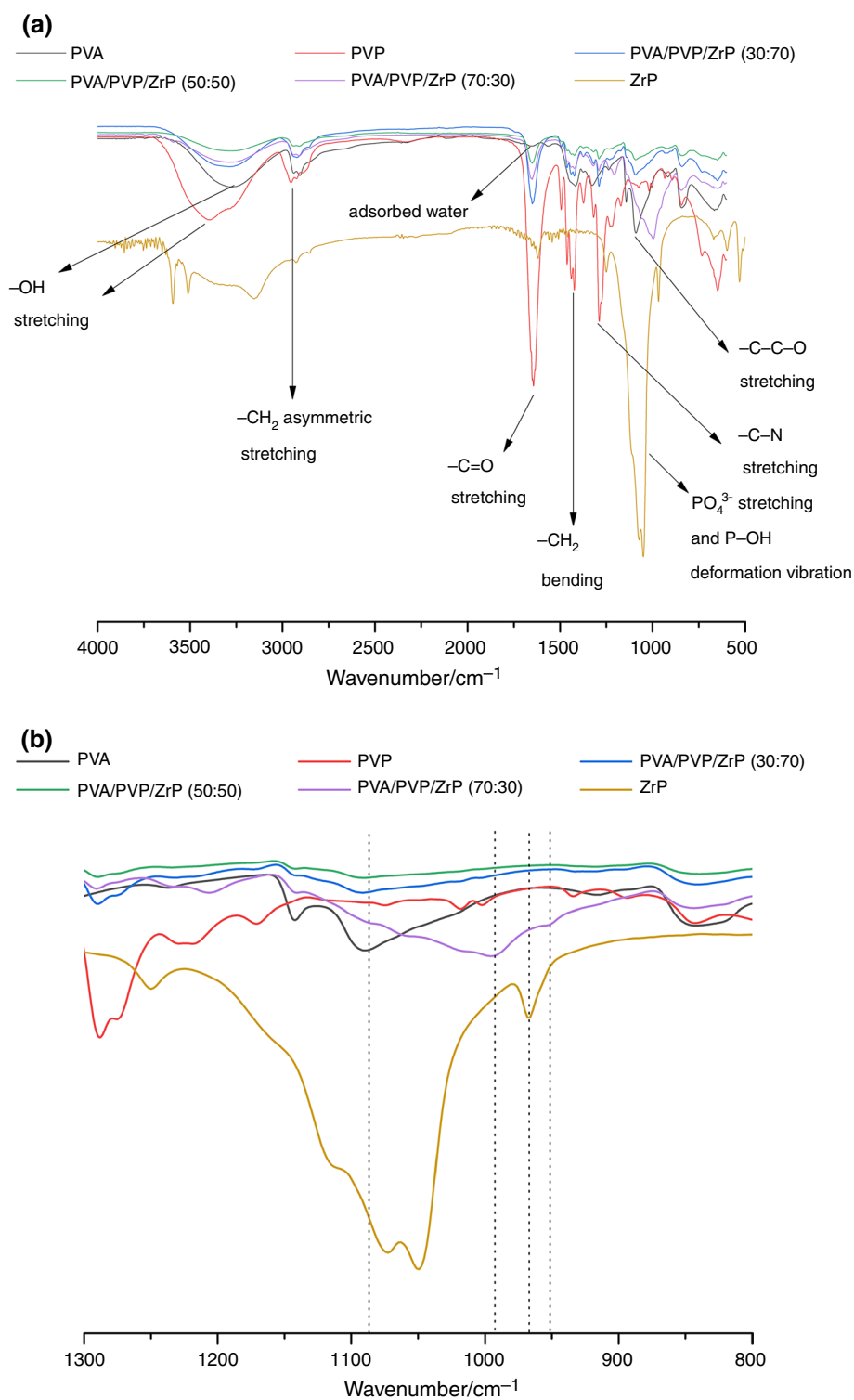


Fig. 2 Schematic representation of hydrogen bond formation between PVA and ZrP

Fig. 3 Full FTIR spectra (a) and spectral region 1300–800 cm^{-1} (b) of the PVA, PVP, ZrP, and PVA/PVP/ZrP nanocomposites



Fourier-transform infrared spectroscopy (FTIR)

Figures 3 show full FTIR spectra and spectral region (1300–800 cm^{-1}) of the samples. They are ratified by works developed on PVA/PVP blends and composites involving the homopolymers and blends [32, 40–44].

Let us focus on evaluating the nanocomposite spectra comparing to the pristine components. At 3500–3000 cm^{-1} , PVP and ZrP change their outline. In this region, they separately present hydrogen bond with water molecules, but when they were mixed together, this interaction was lost. In this spectral region, the nanocomposite spectra resembled the PVA

one [45] as reported by the absorption peak at 1141 cm^{-1} associated with the PVA crystalline portion. Herein, band intensity tends to diminish from the PVA-rich nanocomposite to the poor one composite. The PVA C–C–O stretching at 1088 cm^{-1} was enlarged and sharply shifted to 996 cm^{-1} for the nanocomposite PVA/PVP/ZrP (70/30/2 mass/mass/mass%). Displacement of the PVA C–C–OH stretching from 1100 to 1124 cm^{-1} in PVA/PVP blend doped with CdCl_2 was described by Baraker and Lobo [46]. The authors attributed this change to the involvement of PVA hydroxyl group in the reduction process, conjugation, and co-ordination among Cd^{2+} ions and OH^- ions. The ZrP absorptions at 1250 , 1070 , 1050 , and 970 cm^{-1} are superimposed by PVA ones. The band at 970 was shifted to 950 cm^{-1} . Highly electronegative, the pyrrolidone group attached to the PVP structure is a good proton acceptor [15]. It was expected its intense interaction with PVA and ZrP due to its ability to form intramolecular/intermolecular hydrogen bond. If it happens, it was less predominant than PVA/ZrP interaction since there was no displacement in PVP main absorptions bands. As postulated in the X-ray diffraction evaluation, the changes that occurred in the FTIR spectra were mostly due to the strong interaction between PVA hydroxyl groups and P–OH of the ZrP.

Thermogravimetry (TGA) and differential scanning calorimetry (DSC)

Thermogravimetry (TGA)

Figure 4 presents the loss mass and derivative curves of the nanocomposites. Table 3 illustrates the thermal properties. PVA showed three degradation steps. The first one was attributed to the release of adsorbed water. The intermediate step was associated with the dehydroxylation reaction of the side hydroxyl groups. The last one was assigned as backbone degradation. Betti reported two degradation steps of PVA in oxidative atmosphere [47]. Three degradation steps were observed by Ravindra et al. using nitrogen as carrying gas in their work on PVA/PVP/vanillin composites [48]. In this work, two degradation steps were registered for PVP. They were ascribed to the adsorbed water and polymer backbone degradation, respectively. The works of Elashmawi and Abdel Baiethn [49], Mendes et al. and Abou Taleb endorsed the findings [32, 43]. Similar to PVA, all nanocomposites curves exhibited three degradation steps. By analogy, the initial and intermediate steps were related to the release of adsorbed water and dehydroxylation reaction of PVA chains, respectively. The final one was associated with the degradation of chain backbone of PVA and PVP, respectively. The effect of filler on blends thermal characteristics was evaluated by T_{50} —temperature in that 50% of loss mass happened—and T_{max} —temperature of the maximum degradation rate. Despite the blend composition, the presence of ZrP displaced T_{50} to higher temperature.

For PVA-rich blend, the ZrP showed strong effect on T_{max} dislocated it to higher temperature, while the blend rich in PVP the maintenance of T_{max} was noticed. Mondal et al. [42] pointed out an improvement in PVA thermal stability in the presence of PVP due to hydrogen bonding. The enhancement of thermal stability of PVA/PVP blend filled with LiBr was reported by Abdelrazek an co-author [50]. In their investigation of PVA/PVP/hydroxyapatite composite, Elashmawi et al. observed the decrease in thermal stability of the blend system [49]. Independent on the blend composition, the PVA component was strongly affected by ZrP. The step of dehydroxylation and backbone degradation was shifted to a higher temperature. The results agree with those of the WAXD and FTIR sections.

Differential scanning calorimetry (DSC)

Figure 5 and Table 4 show the third heating cycle DSC curves and calorimetric properties of the PVA, PVP, and nanocomposites, respectively. PVA curve exhibits some disturbance below $100\text{ }^\circ\text{C}$ attributed to its glass transition temperature (T_g) and also crystalline melting temperature T_m at $226\text{ }^\circ\text{C}$. Around 150 – $200\text{ }^\circ\text{C}$, the fluctuation observed in the PVP curve was associated with its T_g . Between 100 and $150\text{ }^\circ\text{C}$, all nanocomposites curves presented fluctuations assigned as T_g for the blend. The glass transition temperature of all samples will be evaluated in detail in the DMA topic. Concerning to PVA cold crystallization temperature (T_{cc}), it was seen at $200\text{ }^\circ\text{C}$. For the nanocomposites, this transition only was detected around $190\text{ }^\circ\text{C}$ for PVA/PVP/ZrP 70/30/2 mass/mass/mass%. PVA melting peak appeared for PVA/PVP/ZrP with 70 and 50 mass% of poly(vinyl alcohol). In the investigation on PVA/PVP (50/50 mass/mass%) blend, Abdelrazek et al. [50] reported that PVA melting peak did not appear by addition of lithium bromide. Razzak and co-workers [51] revealed the decrease in PVA melting temperature as the blend was enriched by PVP. Concerning to PVA crystallinity degree, it decreased in the nanocomposites with 70 and 50 mass% of PVA while that one with lower amount of PVA was amorphous. The addition of Na-montmorillonite as filler in PVA/PVP blend induced the decrease in PVA crystallinity degree as pointed out by Mondal et al. [42]. Lewandowska [28] studied miscibility of blend based on crystalline polymer (PVA) and amorphous one (PVP). Its results indicated the lowering of PVA crystallinity degree according to the PVP amount. Patil et al. found an increase in crystallinity degree in PVA/PVP/ CoCl_2 composite by action of cobalt chloride [52]. Although it has been used X-ray diffraction to measure PVA crystallinity degree, Hemalatha et al. pointed out that cupric sulfate increased the amorphousity of the polymeric matrix [53]. Herein, we associate the changes in PVA calorimetric properties with its interaction with P–OH groups of the ZrP. Indeed, this retards the PVA crystallization rate and in the case of the

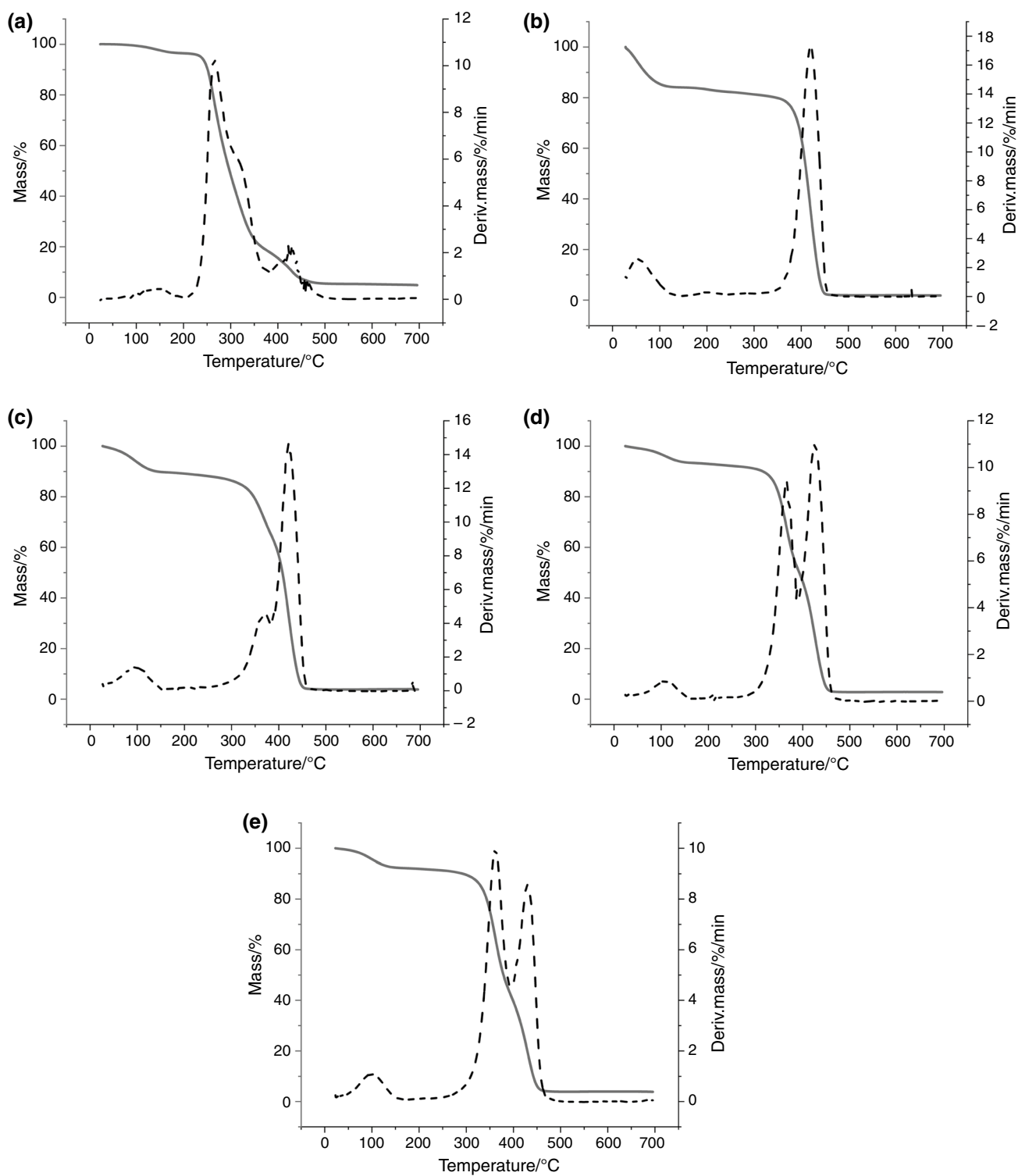


Fig. 4 TGA curves of **a** PVA, **b** PVP, and PVA/PVP/ZrP nanocomposites: **c** 70/30/2, **d** 50/50/2, and **e** 30/70/2

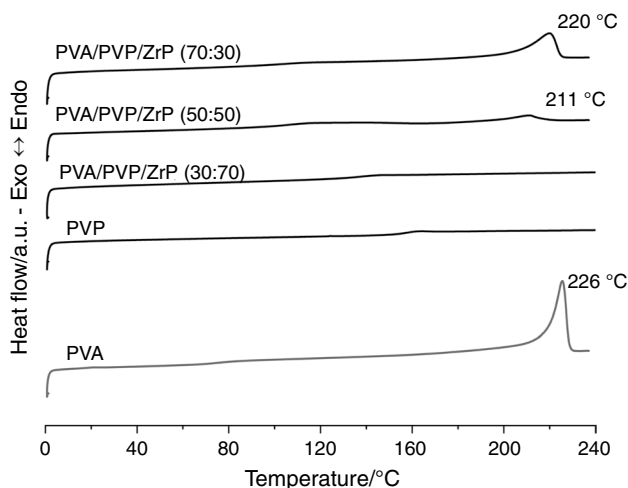
nanocomposite with the lower content of PVA the crystallization process was avoided. This behavior could induce the improvement in the blend miscibility.

Dynamic mechanical analysis (DMA)

Figure 6 displays the storage modulus (E'), loss modulus (E''), and tangent delta ($\tan \delta$) curves of the PVA, PVP, and

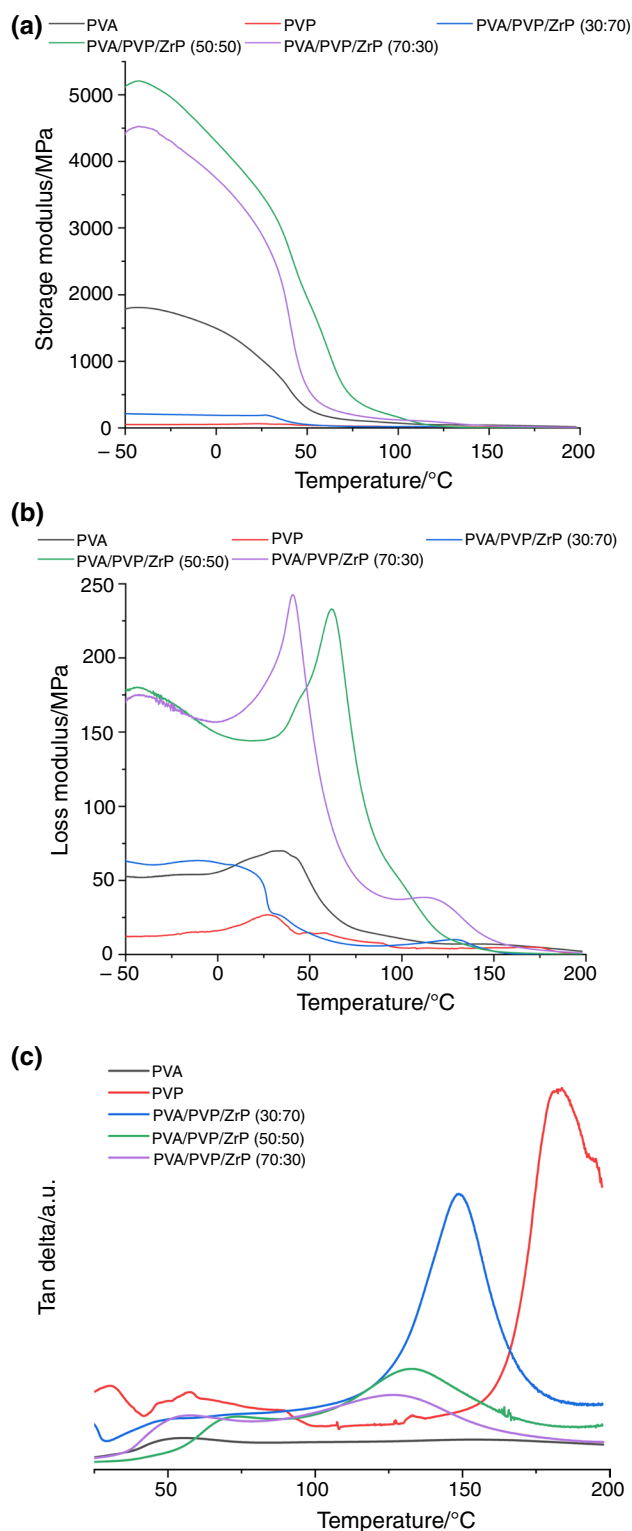
Table 3 TGA data of PVA, PVP and PVA/PVP/ZrP nanocomposites

| Thermal characteristic | PVA | PVP | PVA/PVP/ZrP nanocomposites | | |
|-----------------------------------|-----|-----|----------------------------|---------|---------|
| | | | 70/30 | 50/50 | 30/70 |
| $T_{50}/^{\circ}\text{C}$ | 298 | 411 | 379 | 393 | 408 |
| $T_{\text{max}}/^{\circ}\text{C}$ | 265 | 420 | 361/430 | 367/425 | 371/420 |

**Fig. 5** DSC curves of PVA, PVP, and PVA/PVP/ZrP nanocomposites (third heating scan)**Table 4** Cold crystallization and melting temperatures (T_{cc} and T_{m}) and crystallinity degree (X_{c}) of the PVA, PVP and PVA/PVP/ZrP nanocomposites

| Calorimetric characteristic | PVA | PVP | PVA/PVP/ZrP(2%) nanocomposites | | |
|----------------------------------|-----|-----|--------------------------------|-------|-------|
| | | | 70/30 | 50/50 | 30/70 |
| $T_{\text{cc}}/^{\circ}\text{C}$ | 200 | – | 190 | – | – |
| $T_{\text{m}}/^{\circ}\text{C}$ | 226 | – | 220 | 211 | – |
| X_{c} | 52 | – | 27 | 7,2 | – |

nanocomposites. Table 5 arranges the dynamic-mechanical data. Nanocomposites with 70 and 50 mass% of PVA showed the highest E' values indicating that ZrP acted as reinforcing filler. With 30 mass% of PVA, E' value is located between precursors. With respect to E'' , the behavior was similar. Tangent δ of PVA displays one relaxation peak near to 55 °C associated with its glass transition temperature (T_{g}). There is discrepancy on the assignment of T_{g} value of the 99% hydrolyzed PVA. For PVA supplied by different sources but with similar molar mass and 99% hydrolyzed, Roohani et al. reported two glass transition temperatures (T_{g}) values at 40 and 48 °C [54]. High T_{g} value (92 °C) was registered by Lewandowska in the work on poly(vinyl alcohol)/chitosan mixtures [55].

**Fig. 6** Storage modulus, loss modulus, and tangent delta of PVA, PVP, and PVA/PVP/ZrP nanocomposites

Chiellini assigned the T_{g} of PVA at 27 °C in his investigation on composite based on poly(vinyl alcohol) and sugar cane bagasse [56]. PVA sample annealed at different

Table 5 DMA data of the PVA, PVP, and PVA/PVP/ZrP nanocomposites

| Physics characteristic | PVA | PVP | PVA/PVP/ZrP(2%) nanocomposites | | |
|-----------------------------|-----|-----|--------------------------------|-------|-------|
| | | | 70/30 | 50/50 | 30/70 |
| $T_g/^\circ\text{C}$ —PVA | 55 | — | 57 | 74 | — |
| $T_g/^\circ\text{C}$ —PVP | — | 184 | 126 | 131 | 149 |
| $T_g/^\circ\text{C}$ —Fox | — | — | 93 | 117 | 144 |
| w' PVA | — | — | 0.377 | 0.341 | 0.219 |
| w'' PVP | — | — | 0.021 | 0.192 | — |
| ϵ_{PVA} (%) | — | — | 14.15 | 29.67 | — |
| ϵ_{PVP} (%) | — | — | 7.35 | 22.54 | — |

temperatures showed T_g around 76 and 82 °C as reported by Betzabe Gonzalez-Campos and co-authors [57]. PVP showed its T_g at high temperature (184 °C). Sakurai et al. [58], Feldstein et al. [59], and Hancock et al. [60] published in their works PVP T_g values at 175, 179, and 185 °C, respectively, $\text{Tan}\delta$ curves of PVA/PVP/Zr, 70/30/2 and 50/50/2, presented two T_{gs} related to the PVA and PVP phases. The relaxation values are too different those calculated from Fox's equation. Indeed, these nanocomposites are partially miscible polymeric systems. Sharp and broadened single peak was noticed for PVA/PVP/ZrP 30/70/2 nanocomposite with maximum at 149 °C. This value is quite near of that calculated from Fox's equation (144 °C). Then, it is reasonable to deduce that a miscible polymeric system was reached. Also, there are divergences on the assignments of the glass transition temperature of PVA/PVP blends. Through differential scanning calorimetry (DSC), PVA/PVP (50/50 mass/mass%) blend showed a unique T_g at 98 °C as pointed out by Elashmawi and co-worker [49]. Lewandowska [28] published T_g values of PVA/PVP blend films quite different to each other and with great deviation of the Fox's equation using differential scanning calorimetry and dynamic mechanical analyses. Rajeswari et al. [61] reported T_g at around 60 °C in their study on PVA/PVP 50/50 mass/mass% blend and composites with $\text{CH}_3\text{COONH}_4$ electrolyte. The effect of variable sericin concentration on the properties of PVA/PVP (50/50 mass/mass%) blend was carried out by Ramesan et al. [62]. According to them, the T_g of the blend was located at around 114 °C. Disagreements could be attributed to the variable properties of the precursor polymers, sample preparation, different measurement techniques, erroneous assignments, and so on. Considering our investigation about miscibility interphases, we get in different blends values of ϵ_{PVA} greater than ϵ_{PVP} . This means that the participation effectiveness degree of PVA on PVP-rich phase was superior of that PVP on the PVA-rich phase. Considering the amorphous morphology and lower molar

mass of PVP, we expected the reverse behavior. This could be associated with the strong interaction between PVA and ZrP as previously postulated.

Conclusions

PVA/PVP/ZrP nanocomposites were prepared and the effects of ZrP on the structural, thermal, molecular mobility, and miscibility were assessed. PVA infrared C—C—O absorption peak was shifted to lower wavelength. For any polymer composition, PVA thermal degradation steps were displaced to a higher temperature. Independent on the blend composition, ZrP crystalline arrangement was damaged. PVA calorimetric properties were altered. On the contrary, we expected, the participation effectiveness degree of PVA on PVP-rich phase was superior to that PVP on the PVA-rich phase. Herein, this evidence led to the belief that preferentially the formation of hydrogen bond between PVA and ZrP occurred. Promising results were achieved in the searching for a new material applicable in control drug delivery system.

Acknowledgements The authors thank the Conselho Nacional de Desenvolvimento Científico e Tecnológico (CNPq), Coordenação de Aperfeiçoamento de Pessoal de Nível Superior (CAPES), Finance Code 1 and Universidade Federal do Rio de Janeiro for financial supporting of this work.

References

1. Utracki LA. Polymer blends, vol. 11. Akron: Smithers Rapra Publishing; 2000.
2. Parameswaranpillai J, Siengchin S, George J, Jose S. Shape memory polymers, blends and composites. New York: Springer; 2019.
3. Sedaghat E, Rostami AA, Ghaemy M, Rostami A. Characterization, thermal degradation kinetics, and morphological properties of a graphene oxide/poly (vinyl alcohol)/starch nanocomposite. *J Therm Anal Calorim*. 2018. <https://doi.org/10.1007/s10973-018-7649-1>.
4. Gökmeşe F, Uslu İ, Aytimur A. Preparation and characterization of PVA/PVP nanofibers as promising materials for wound dressing. *Polym-Plast Technol*. 2013. <https://doi.org/10.1080/03602559.2013.814144>.
5. Ragab HM. Spectroscopic investigations and electrical properties of PVA/PVP blend filled with different concentrations of nickel chloride. *Phys B*. 2011. <https://doi.org/10.1016/j.physb.2010.11.030>.
6. Seabra AB, de Oliveira MG. Poly(vinyl alcohol) and poly(vinyl pyrrolidone) blended films for local nitric oxide release. *Biomaterials*. 2004. <https://doi.org/10.1016/j.biomaterials.2003.10.035>.
7. Yu H, Xu X, Chen X, Lu T, Zhang P, Jing X. Preparation and antibacterial effects of PVA-PVP hydrogels containing silver nanoparticles. *J Appl Polym Sci*. 2006. <https://doi.org/10.1002/app.24835>.
8. Huang K, Hsiao C, Nien Y, Lin J. Synthesis, characterization, and application of PVP/PAM copolymer. *J Appl Polym Sci*. 2005. <https://doi.org/10.1002/app.22795>.

9. Szczerba M, Środoń J, Skiba M, Derkowski A. One-dimensional structure of exfoliated polymer-layered silicate nanocomposites: a polyvinylpyrrolidone (PVP) case study. *Appl Clay Sci.* 2010. <https://doi.org/10.1016/j.clay.2009.10.015>.
10. Loria-Bastarrachea MI, Herrera-Kao W, Cauich-Rodríguez JV, Cervantes-Uc J, Vázquez-Torres H, Ávila-Ortega A. A TG/FTIR study on the thermal degradation of poly(vinyl pyrrolidone). *J Therm Anal Calorim.* 2010. <https://doi.org/10.1007/s10973-010-1061-9>.
11. Shirini F, Goli-Jolodar O, Akbari M, Seddighi M. Preparation, characterization, and use of poly(vinylpyrrolidonium) hydrogen phosphate (PVP-H₂H₂PO₄) as a new heterogeneous catalyst for efficient synthesis of 2-amino-tetrahydro-4H-pyrans. *Res Chem Intermed.* 2015. <https://doi.org/10.1007/s11164-015-2312-y>.
12. Wang Q, Hikima T, Tojo K. Skin penetration enhancement by the synergistic effect of supersaturated dissolution and chemical enhancers. *J Chem Eng Jpn.* 2003. <https://doi.org/10.1252/jcej.36.92>.
13. Nishio Y, Haratani T, Takahashi T. Miscibility and orientation behavior of poly(vinyl alcohol)/poly(vinyl pyrrolidone) blends. *J Polym Sci Pol Phys.* 1990. <https://doi.org/10.1002/polb.1990.090280308>.
14. Baraker BM, Lobo B. Multistage thermal decomposition in films of cadmium chloride-doped PVA–PVP polymeric blend. *J Therm Anal Calorim.* 2018. <https://doi.org/10.1007/s10973-018-7289-5>.
15. Eisa WH, Abdel-Moneam YK, Shabaka AA, Hosam AE. In situ approach induced growth of highly monodispersed Ag nanoparticles within free standing PVA/PVP films. *Spectrochim Acta A.* 2012. <https://doi.org/10.1016/j.saa.2012.03.085>.
16. Qian X, Yin J, Feng S, Liu S, Zhu Z. Preparation and characterization of polyvinylpyrrolidone films containing silver sulfide nanoparticles. *J Mater Chem.* 2001. <https://doi.org/10.1039/B103708K>.
17. Lee S, Oh C, Lee D. Large improvement in the mechanical properties of polyurethane nanocomposites based on a highly concentrated graphite nanoplate/polyol masterbatch. *Nanomaterials.* 2019. <https://doi.org/10.3390/nano9030389>.
18. Fang F, Ran S, Fang Z, Song P, Wang H. Improved flame resistance and thermo-mechanical properties of epoxy resin nanocomposites from functionalized graphene oxide via self-assembly in water. *Compos B Eng.* 2019. <https://doi.org/10.1016/j.compositesb.2019.01.086>.
19. Yang Y, Liu C, Wu H. Preparation and properties of poly(vinyl alcohol)/exfoliated α -zirconium phosphate nanocomposite films. *Polym Test.* 2009. <https://doi.org/10.1016/j.polymertesting.2008.12.008>.
20. Mendes LC, Silva DF, Araujo LJP, Lino AS. Zirconium phosphate organically intercalated/exfoliated with long chain amine). *J Therm Anal Calorim.* 2014. <https://doi.org/10.1007/s10973-014-4056-0>.
21. Sue HJ, Gam KT, Bestaoui N, Spurr N, Clearfield A. Epoxy nanocomposites based on the synthetic α -zirconium phosphate layer structure. *Chem Mater.* 2004. <https://doi.org/10.1021/cm030441s>.
22. Boo WJ, Sun L, Liu J, Clearfield A, Sue H. Effective intercalation and exfoliation of nanoplatelets in epoxy via creation of porous pathways. *J Phys Chem C.* 2007. <https://doi.org/10.1021/jp072227n>.
23. Garcia EE, Freitas DFS, Cestari SP, Coval DR, Mendes LC, Albitres GAV. Zirconium phosphate changing hygroscopicity of polyamide-6 in nanocomposites PA-6/ZrP. *J Therm Anal Calorim.* 2019. <https://doi.org/10.1007/s10973-019-08396-1>.
24. Alberti G. Syntheses, crystalline structure, and ion-exchange properties of insoluble acid salts of tetravalent metals and their salt forms. *Acc Chem Res.* 1978. <https://doi.org/10.1021/ar50124a007>.
25. Chowreddy RR, Nord-Varhaug K, Rapp F. Recycled polyethylene terephthalate/carbon nanotube composites with improved processability and performance. *J Mater Sci.* 2018. <https://doi.org/10.1007/s10853-018-2014-0>.
26. Martins-Franchetti SM, Campos A, Egerton TA, White JR. Structural and morphological changes in Poly(caprolactone)/poly(vinyl chloride) blends caused by UV irradiation. *J Mater Sci.* 2007. <https://doi.org/10.1007/s10853-007-2210-9>.
27. Campos A, Marconato J, Martins-Franchetti S. Biodegradation of blend films PVA/PVC, PVA/PCL in soil and soil with landfill leachate. *Braz Arch Biol Techn.* 2011. <https://doi.org/10.1590/S1516-89132011000600024>.
28. Lewandowska K. The miscibility of poly(vinyl alcohol)/poly(N-vinylpyrrolidone) blends investigated in dilute solutions and solids. *Eur Polym J.* 2005. <https://doi.org/10.1016/j.eurpolymj.2004.08.016>.
29. Santana OO, Maspoch ML, Martínez AB. Polycarbonate/acrylonitrile-butadiene-styrene blends: miscibility and interfacial adhesion. *Polym Bull.* 1998. <https://doi.org/10.1007/s002890050424>.
30. Al-Jabareen A, Illescas S, Maspoch ML, Santana OO. Effects of composition and transesterification catalysts on the physicochemical and dynamic properties of PC/PET blends rich in PC. *J Mater Sci.* 2010. <https://doi.org/10.1007/s10853-010-4753-4>.
31. Mendes LC, Pereira PSC. Solid state polymerization: its action on thermal and rheological properties of PET/PC reactive blends. *Polimeros.* 2013. <https://doi.org/10.4322/polimeros.2013.031>.
32. Mendes LC, Rodrigues RC, Silva EP. Thermal, structural and morphological assessment of PVP/HA composites. *J Therm Anal Calorim.* 2010. <https://doi.org/10.1007/s10973-010-0835-4>.
33. Cheng Y, Chuah GK. The synthesis and applications of α -zirconium phosphate. *Chin Chem Lett.* 2019. <https://doi.org/10.1016/j.ccllet.2019.04.063>.
34. Xiao H, Liu S. Zirconium phosphate (ZrP)-based functional materials: Synthesis, properties and applications. *Mater Des.* 2018. <https://doi.org/10.1016/j.matdes.2018.05.041>.
35. Dal Pont K, Gérard JF, Espuche E. Modification of α -ZrP nanofillers by amines of different chain length: consequences on the morphology and mechanical properties of styrene butadiene rubber based nanocomposites. *Eur Polym J.* 2012. <https://doi.org/10.1016/j.eurpolymj.2011.11.006>.
36. Gardolinski JE, Carrera LCM, Cantão MP, Wypych F. Layered polymer-kaolinite nanocomposites. *J Mater Sci.* 2000. <https://doi.org/10.1023/A:1004820003253>.
37. Fong H, Liu W, Wang C, Vaia RA. Generation of electrospun fibers of nylon 6 and nylon 6-montmorillonite nanocomposite. *Polymer.* 2002. [https://doi.org/10.1016/S0032-3861\(01\)00665-6](https://doi.org/10.1016/S0032-3861(01)00665-6).
38. Wu T, Chen E, Liao C. Polymorphic behavior of nylon 6/saponite and nylon 6/montmorillonite nanocomposites. *Polym Eng Sci.* 2002. <https://doi.org/10.1002/pen.11018>.
39. Chang J, An YU, Cho D, Giannelis EP. Poly(lactic acid) nanocomposites: comparison of their properties with montmorillonite and synthetic mica (II). *Polymer.* 2003. [https://doi.org/10.1016/S0032-3861\(03\)00276-3](https://doi.org/10.1016/S0032-3861(03)00276-3).
40. Abdelrazek EM, Elashmawi IS, Labeeb S. Chitosan filler effects on the experimental characterization, spectroscopic investigation and thermal studies of PVA/PVP blend films. *Phys B.* 2010. <https://doi.org/10.1016/j.physb.2010.01.095>.
41. Afzal HM, Shehzad F, Zubair M, Bakather OY, Al-Harthi MA. Influence of microwave irradiation on thermal properties of PVA and PVA/graphene nanocomposites. *J Therm Anal Calorim.* 2019. <https://doi.org/10.1007/s10973-019-08419-x>.
42. Mondal D, Mollick MM, Bhowmick B, Maity D, Bain MK, Rana D, et al. Effect of poly(vinyl pyrrolidone) on the morphology and physical properties of poly(vinyl alcohol)/sodium montmorillonite

- nanocomposite films. *Prog Nat Sci-Mater*. 2013. <https://doi.org/10.1016/j.pnsc.2013.11.009>.
43. Abou Taleb MH. Thermal and spectroscopic studies of poly(N-vinyl pyrrolidone)/poly(vinyl alcohol) blend films. *J Appl Polym Sci*. 2009. <https://doi.org/10.1002/app.30082>.
 44. Shi Y, Xiong D, Liu Y, Wang N, Zhao X. Swelling, mechanical and friction properties of PVA/PVP hydrogels after swelling in osmotic pressure solution. *Mater Sci Eng C*. 2016. <https://doi.org/10.1016/j.msec.2016.04.042>.
 45. Peppas NA. Infrared spectroscopy of semicrystalline poly(vinyl alcohol) networks. *Macromol Chem Phys*. 1977. <https://doi.org/10.1002/macp.1977.021780228>.
 46. Baraker BM, Lobo B. UV irradiation induced microstructural changes in CdCl₂ doped PVA–PVP blend. *J Mater Sci Mater El*. 2017. <https://doi.org/10.1007/s10854-017-8355-7>.
 47. Betti NA. Thermogravimetric analysis on PVA/PVP blend under air atmosphere. *Eng Technol J*. 2016;34:2433–41.
 48. Ravindra C, Sarswati M, Sukanya G, Shivalila P, Soumya Y, Deepak K. Tensile and thermal properties of poly(vinyl pyrrolidone)/vanillin incorporated poly (vinyl alcohol) films. *Res J Phys Sci*. 2015;3:1–6.
 49. Elashmawi IS, Abdel Baieth HE. Spectroscopic studies of hydroxyapatite in PVP/PVA polymeric matrix as biomaterial. *Curr Appl Phys*. 2012. <https://doi.org/10.1016/j.cap.2011.05.011>.
 50. Abdelrazek EM, Elashmawi IS, El-khodary A, Yassin A. Structural, optical, thermal and electrical studies on PVA/PVP blends filled with lithium bromide. *Curr Appl Phys*. 2010. <https://doi.org/10.1016/j.cap.2009.08.005>.
 51. Razzak MT, Zainuddin Erizal, Dewi SP, Lely H, Taty E. The characterization of dressing component materials and radiation formation of PVA–PVP hydrogel. *Radiat Phys Chem*. 1999. [https://doi.org/10.1016/S0969-806X\(98\)00320-X](https://doi.org/10.1016/S0969-806X(98)00320-X).
 52. Patil RV, Ranganath MR, Lobo B. Microstructural studies on cobalt chloride doped PVA–PVP blend. *Int J Chem Technol Res*. 2014;6:1852–4.
 53. Hemalatha K, Somashekarappa H, Somashekar R. Micro-structure, AC conductivity and spectroscopic studies of cupric sulphate doped PVA/PVP polymer composites. *Adv Mater Phys Chem*. 2015. <https://doi.org/10.4236/ampc.2015.510041>.
 54. Roohani M, Habibi Y, Belgacem NM, Ebrahim G, Karimi AN, Dufresne A. Cellulose whiskers reinforced polyvinyl alcohol copolymers nanocomposites. *Eur Polym J*. 2008. <https://doi.org/10.1016/j.eurpolymj.2008.05.024>.
 55. Lewandowska K. Miscibility and thermal stability of poly(vinyl alcohol)/chitosan mixtures. *Thermochim Acta*. 2009. <https://doi.org/10.1016/j.tca.2009.04.003>.
 56. Chiellini E, Cinelli P, Solaro R, Laus M. Thermomechanical behavior of poly(vinyl alcohol) and sugar cane bagasse composites. *J Appl Polym Sci*. 2004. <https://doi.org/10.1002/app.13649>.
 57. Betzabe Gonzalez-Campos J, Garcia-Carvajal ZY, Prokhorov E, Luna-Barcenas JG, Mendoza-Duarte ME, Lara-Romero J, del Rio RE, Sanchez IC. Revisiting the thermal relaxations of poly(vinyl alcohol). *J Appl Polym Sci*. 2012. <https://doi.org/10.1002/app.33615>.
 58. Sakurai K, Maegawa T, Takahashi T. Glass transition temperature of chitosan and miscibility of chitosan/poly(N-vinyl pyrrolidone) blends. *Polymer*. 2000. [https://doi.org/10.1016/S0032-3861\(00\)00067-7](https://doi.org/10.1016/S0032-3861(00)00067-7).
 59. Feldstein MM, Roos A, Chevallier C, Creton C, Dormidontova EE. Relation of glass transition temperature to the hydrogen bonding degree and energy in poly(N-vinyl pyrrolidone) blends with hydroxyl-containing plasticizers: 3. Analysis of two glass transition temperatures featured for PVP solutions in liquid poly(ethylene glycol). *Polymer*. 2003. [https://doi.org/10.1016/S0032-3861\(03\)00046-6](https://doi.org/10.1016/S0032-3861(03)00046-6).
 60. Hancock BC, Shamblin SL, Zografi G. Molecular mobility of amorphous pharmaceutical solids below their glass transition temperatures. *Pharm Res*. 1995. <https://doi.org/10.1023/A:1016292416526>.
 61. Rajeswari N, Selvasekarapandian S, Karthikeyan S, Sanjeeviraja C, Iwai Y, Kawamura J. Structural, vibrational, thermal, and electrical properties of PVA/PVP biodegradable polymer blend electrolyte with CH₃–COONH₄. *Ionics*. 2013. <https://doi.org/10.1007/s11581-012-0838-1>.
 62. Ramesan MT, Athira VK, Jayakrishnan P, Gopinathan C. Preparation, characterization, electrical and antibacterial properties of sericin/poly(vinyl alcohol)/poly(vinyl pyrrolidone) composites. *J Appl Polym Sci*. 2016. <https://doi.org/10.1002/app.43535>.

Publisher's Note Springer Nature remains neutral with regard to jurisdictional claims in published maps and institutional affiliations.